Molecular Catalysis 522 (2022) 112247

Contents lists available at ScienceDirect

Molecular Catalysis

journal homepage: www.journals.elsevier.com/molecular-catalysis

Mechanism of transfer hydrogenation of carbonyl compounds by zirconium and hafnium-containing metal-organic frameworks

Mohammad Shahinur Rahaman [a], Sarttrawut Tulaphol [b], Md. Anwar Hossain [a], Matthew C. Mulvehill [a], Joshua M. Spurgeon [c], Thana Maihom [d,*], Noppadon Sathitsuksanoh [a,*]

[a] Department of Chemical Engineering, University of Louisville, Louisville, KY 40292, USA
[b] Sustainable Polymer & Innovative Composite Materials Research Group, Department of Chemistry, Faculty of Science, King Mongkut's University of Technology Thonburi, Bangkok 10140, Thailand
[c] Conn Center for Renewable Energy, University of Louisville, Louisville, KY 40292, USA
[d] Department of Chemistry, Faculty of Liberal Arts and Science, Kasetsart University, Kamphaeng Saen Campus, Nakhon Pathom 73140, Thailand

ARTICLE INFO

Keywords:
Carbonyl
Transfer hydrogenation
Meerwein–Ponndorf–Verley
Metal-organic frameworks
Biomass

ABSTRACT

Liquid phase catalytic hydrogenation is essential to produce platform chemicals from biomass-derived carbonyl compounds. Carbonyl compounds can be upgraded to corresponding alcohols by catalytic transfer hydrogenation using hydrogen-donor solvents and mild reaction conditions. The challenge in transfer hydrogenation is the development of selective, active, and reusable catalysts. Here we show the chemical pathway of transfer hydrogenation of benzaldehyde by Hf- and Zr-containing MOF-808 and UiO-66 catalysts. MOF-808(Hf) was the most selective catalyst with 95% selectivity to benzyl alcohol at 99% conversion. Furthermore, the quantum calculations revealed that the transfer hydrogenation by MOF-808(Hf) proceeded by Meerwein–Ponndorf–Verley (MPV) reduction, which resulted in high selectivity and conversion. These findings of the effects of metal and acid sites of these MOFs enable maximizing the selectivity for transfer hydrogenation. Moreover, understanding these effects provide opportunities for these MOFs in other biomass conversion reactions.

1. Introduction

Production of fuels and chemicals from renewable biomass reduces reliance on fossil fuels [1] and mitigates global warming by reducing CO_2 emissions [2]. Biomass-derived compounds such as furfural, 5-hydroxymethylfurfural, and benzaldehyde contain oxygens in carbonyl groups and unsaturated C=C bonds. Catalytic hydrogenation is important to convert biomass-derived carbonyl compounds into high-value chemicals, such as γ-valerolactone [3], di-hydroxy-methyl-tetrahydrofuran [4], tetrahydrofurfuryl alcohol [5], and hexitol [6]. Classic hydrogenation is based on metal catalysts, such as Pd/C [7], Pt/C [4], Rh/C [8,9], Ni–Pd/SiO_2 [10], Au/Al_2O_3 [11], Ni/Al_2O_3 [12], Cu/Al_2O_3 [13], Pt/Al_2O_3 [14], PtSn/Al_2O_3 [15], Ir/TiO_2 [16], and molecular H_2. However, hydrogenation using molecular H_2 poses cost and safety concerns [17]. In addition, selective hydrogenation of the carbonyl group (C=O) is problematic because hydrogenation of C=C bonds is thermodynamically favorable compared with C=O bonds, and C=C bond hydrogenation produces undesired products [18,19]. Therefore, many investigators have investigated catalytic transfer hydrogenation to overcome these challenges.

Catalytic transfer hydrogenation that uses hydrogen-donor solvents instead of molecular H_2 is an alternative approach to converting carbonyl compounds into corresponding alcohols [20]. Transfer hydrogenation can occur by: (1) direct hydrogen transfer from alcohol to the carbonyl group at the active metal site of a catalyst, and (2) a cascade of metal hydride formation and carbonyl reduction by Meerwein–Ponndorf–Verley (MPV) by Lewis acid catalysts. MPV reduction is promising for hydrogenation of biomass-derived carbonyls because of its high chemoselectivity, mild reaction conditions, and scalability [21,22]. Lewis acidic Hf-, Zr-, and Sn-containing zeolites catalyzed MPV reduction [23–30]. However, synthesis of these zeolites entails complex [31], and time-consuming [32] procedures and the use of hazardous reagents (e.g., HF) [33].

Recently, Hf- and Zr-containing metal-organic frameworks (MOFs), especially MOF-808 and UiO-66 frameworks [34–39], have been shown to catalyze transfer hydrogenation of biomass-derived carbonyl compounds, such levulinic acid [40], furfural [35,41-43], ethyl levulinate [44,45], cinnamaldehyde [46]. For example, Mautschke et al. [37]

---

* Corresponding authors.
E-mail addresses: faastnm@ku.ac.th (T. Maihom), N.sathitsuksanoh@louisville.edu (N. Sathitsuksanoh).

https://doi.org/10.1016/j.mcat.2022.112247
Received 14 January 2022; Received in revised form 17 March 2022; Accepted 20 March 2022

showed that MOF-808(Zr) had a better catalytic performance for MPV of carbonyl compounds compared with UiO-66(Zr). Rojas-Buzo et al. [35] proposed that MOF-808(Hf) catalyzed transfer hydrogenation by a direct hydrogen transfer pathway. In contrast, Lin et al. [36] suggested that MOF-808(Hf) catalyzed MPV reduction. Although they proposed the MPV mechanism by MOF-808(Hf), the effect of linkers and dispersion interactions on the proposed mechanism remained unknown. Thus, still to be determined are the mechanism of transfer hydrogenation by MOF-808 and UiO-66 and the effect of Zr and Hf metal clusters.

Here, we evaluated the catalytic performance of Zr- and Hf-containing MOF-808 and UiO-66 catalyst for transfer hydrogenation of benzaldehyde in 2-propanol at 100 °C. Next, we combined experimental results and density functional theory to elucidate the mechanism by which Hf- and Zr-containing MOFs activate carbonyl compounds during transfer hydrogenation. Our results demonstrated that MOF-808 activated carbonyl groups by MPV, whereas UiO-66 activated carbonyls by direct transfer hydrogenation. Moreover, the Lewis acidic MOF-808(Hf) was the most active and selective to transfer hydrogenation (MPV) of benzaldehyde to benzyl alcohol. In addition, MOF-808(Hf) reduced other biomass-derived carbonyl compounds to corresponding alcohols with >89% selectivity with minimal side reactions. Furthermore, creating defect sites through adding a modulator (formic acid) during MOF-808(Hf) synthesis enhanced its selectivity to alcohol. This study provided an insight into the development of active and selective Lewis acidic MOF catalysts for the transfer hydrogenation of biomass-derived carbonyl compounds.

2. Materials and Methods

2.1. Materials

All chemicals were used as received unless otherwise noted. **Table S1** lists their CAS numbers, purity, and manufacturers (*Supplementary Information, Page S3*)**.**

2.2. Synthesis of metal-organic frameworks

UiO-66(Zr) [47], UiO-66(Hf) [48], MOF-808(Zr) [35], and MOF-808 (Hf) [35] were synthesized using a solvothermal method with a slight modification. The detailed synthesis procedures are described in *the Supplementary Information (Page S4)*.

2.3. Characterization of the catalyst

The physiochemical properties of the MOFs were determined by X-ray diffraction (XRD), N_2 adsorption-desorption, Diffuse reflectance infrared Fourier transform spectroscopy (DRIFTS), Fourier-transform infrared spectroscopy (FTIR), and thermogravimetric analysis (TGA). The metal content was determined by inductively coupled plasma-optical emission spectroscopy (ICP-OES).

2.3.1. X-ray diffraction

X-ray diffraction (XRD) analysis of samples was conducted on a Bruker D8 Discover diffractometer (Billerica, MA, USA) using CuKα radiation in the 2θ range from 10° to 40° with 0.5 seconds/step. Samples of 200 mg were used in each analysis.

2.3.2. N_2 adsorption-desorption

The N_2 adsorption-desorption was measured by a Micromeritics Tristar (Norcross, GA, USA) instrument to calculate the surface area, pore size, and pore volume. The function of TriStar was verified with reference materials (Micromeritics). Before the measurement, the sample was pretreated at 150 °C for 3 h using a Micromeritics FlowPrep with sample degasser (Norcross, GA, USA). The surface area, S_{BET}, was determined from N_2 isotherms by Brunauer–Emmett–Teller equation (BET) at -196.1 °C [24,25]. The BET surface area was calculated for the range of relative pressures between 0.05 and 0.3. The pore volume was estimated from the N_2 desorption values according to the Barrett–Joyner–Halenda (BJH) model [26]. The pore volume was calculated as the uptake (cm^3/g) at a relative pressure of 0.95. We measured the average pore size of the samples by the BJH model [27,28].

2.3.3. Thermogravimetric analysis

To determine the thermal stability of synthesized MOFs, thermogravimetric analysis (TGA) was performed on an SDT Q600 TA instrument (New Castle, DE, USA). In short, ~20 mg of the sample was placed in a cylindrical alumina crucible and heated in the air from ambient temperature to 700 °C with a heating rate of 10 °C/min under N_2 flow (100 mL/min). The change in weight of MOF samples was used to determine the moisture content, decomposition of the linkers, and formation of metal oxides.

2.3.4. Inductively coupled plasma-optical emission spectroscopy

The metal content of the samples was determined by inductively coupled plasma-optical emission spectroscopy (ICP-OES). Measurements were performed using a 100 mg sample dissolved in 10 mL of nitric acid. Heating was used to ensure that the sample was completely dissolved. Once cooled, the sample was further diluted to 25 mL with double distilled water. Measurements were acquired on a Varian 720-ES spectrometer equipped with a seaspray nebulizer and cyclonic class spray chamber. Parameters included a sample intake of 1 mL/min, argon plasma flow rate of 15 L/min, and an auxiliary gas (Ar) flow rate of 1.5 L/min. The instrument was calibrated with certified reference materials (CRMs) by VHG (LGC Standards Ltd., Teddington, UK).

2.3.5. Fourier-transform infrared spectroscopy

Infrared spectra of samples were recorded on a JASCO Fourier transform infrared (FTIR) spectrometer (Easton, MD, USA), equipped with an attenuated total reflection stage (ATR). Samples of ~5 mg were used in each analysis. The samples were scanned between 400 and 4000 cm^{-1} at a 4 cm^{-1} resolution. Spectra were collected using deuterated triglycine sulfate (DTGS) detector averaging 256 scans.

2.3.6. Diffuse reflectance infrared Fourier transform spectroscopy

Diffuse reflectance infrared Fourier transform spectroscopy (DRIFTS) with adsorbed pyridine was performed to characterize the acid sites. The temperature-programmed desorption was conducted using the JASCO FTIR equipped with a high-temperature DiffuseIR™ cell (PIKE Technology, WI, USA). The sample treatment and DRIFTS experiments with temperature-programmed desorption were described elsewhere with a slight modification [49]. Briefly, the MOF sample (~5 mg) was placed in a cylindrical alumina crucible and treated in N_2 gas (50 mL/min) at 150 °C for 60 min unless otherwise noted. After the pretreatment, the sample was cooled to 30 °C, and the IR spectrum of fresh catalyst was recorded as the background spectrum. The samples were then saturated with pyridine vapor in a low concentration of N_2 gas (50 mL/min). Then the physisorbed pyridine was removed by flushing with N_2 gas (50 mL/min) at 150 °C for 30 min before recording the DRIFT spectra. All spectra were recorded with 256 scans in the range between 4000–400 cm^{-1} at a 4 cm^{-1} resolution. The amount of Lewis acid sites at each desorption temperature was calculated from the integrated area of bands (after background subtraction) of adsorbed pyridine at 1012, 1043, and 1070 cm^{-1} [50].

The Brønsted acid properties of MOFs were determined by measuring the pH change of methanol in which MOFs were suspended, as described [34,51,52]. Briefly, 8 mg MOFs were suspended in 24 mL methanol with constant stirring at ambient temperature before pH measurement. The selected sample amount of 8 mg was based on previous experiments in which the amount of MOFs was varied; we found that 8 mg MOF was sufficient such that the measured pH was independent of the amount of solid. The pH was measured with a gel-filled, double junction electrode (Milwaukee Instruments, Inc., Rocky Mount, NC, USA). The electrode was calibrated with the pH 4, 7, and 9 buffers. All measurements were conducted in triplicate.

2.4. Transfer hydrogenation of benzaldehyde

Reactions were performed in 15 mL glass pressure vials in an oil bath. Typically, benzaldehyde, 2-propanol, and catalysts were added to the pressure vial, sealed, and stirred at the desired temperature. The reactor vessel contained three mol% of the desired catalyst, 1% weight of benzaldehyde dissolved in 2-propanol, and 0.25% weight of hexadecane added as an internal standard. The benzaldehyde conversion and product yield were calculated based on the internal standard. The reaction was stopped by quenching in a cold-water bath, then adding ethyl acetate (5 mL) to dissolve the remaining benzaldehyde and products. The solution was centrifuged, and the solid catalyst was removed. The liquid sample was then diluted with ethyl acetate before analysis.

2.5. Product analysis and quantification

The reactants and products were analyzed by a gas chromatograph (7890B GC) (Agilent Technologies, Santa Clara, CA, USA) equipped with a mass spectrometer and flame ionization detector (FID) for product identification and quantification, respectively. A DB-1701 column (30 m x 0.25 mm x 0.25 µm, Agilent Technologies, Santa Clara, CA, USA) was used for product separation with the following parameters: injection temperature 275 °C and FID detector temperature 300 °C; split ratio 1:50. The temperature program started at 50 °C with a heating rate of 8 °C/min to 200 °C. The conversion of benzaldehyde, product yield, and product selectivity were calculated using the following equations:

$$\textbf{Conversion}\ (\%) = \frac{\textbf{mole of benzaldehyde reacted}}{\textbf{initial mole of benzaldehyde}}\textbf{x100}$$

$$\textbf{Product yield}\ (\%) = \frac{\textbf{mole of product generated}}{\textbf{initial mole of benzaldehyde}}\textbf{x100}$$

$$\textbf{Product selectivity}\ (\%) = \frac{\textbf{Product yield}}{\textbf{Conversion}}\textbf{x100}$$

2.6. Computational details

Fig. S1 depicts the cluster models used to represent the MOF-808(Zr/Hf) and UiO-66(Zr/Hf). These cluster models were constructed from their optimized periodic structures. The cluster model of MOF-808 consisted of one zirconium or hafnium oxide node with six benzene-1,3,5-tricarboxylate (BTC) coordinating linkers. In addition, an open Lewis acidic site of MOF-808 formed by removing an external water molecule was considered in the present work [56]. For UiO-66, the cluster involved one hafnium oxide node connected to twelve BTC linkers.

All structure optimizations were calculated from density functional theory (DFT) using the M06-L [57] density function as implemented in the code Gaussian 16 Revision B.01 [58]. The 6-31G(d,p) basis set was employed for the O, C, and H atoms, whereas the Zr and Hf atoms were described by the double-ζ of the Stuttgart-Dresden pseudopotential (SDD). During geometry optimizations, the entire cluster model except for the para-C atoms of benzoate linkers was allowed to relax. Vibrational frequency calculations were performed to identify the nature of all the stationary states along the reaction coordinate. The natural bond orbit method [59] was used to determine orbital overlapping, partial charges, and population analysis.

The difference in charge transfer (DCT) from the catalytic sites to the adsorbed benzaldehyde molecule between the adsorption and transition state complexes was calculated as follows:

$$\Delta CT = q\left(TS_{benzaldehyde}\right) - q\left(TS_{co-adsorbed\ benzaldehyde}\right)$$

where q(TS_benzaldehyde) and q(TS_co-adsorbed benzaldehyde) represented net charges of the benzaldehyde molecule in the transition state and benzaldehyde in the co-adsorption state (co-adsorption of benzaldehyde and 2-propanol molecules), respectively.

3. Results

Initially, we screened 14 metal triflates to identify active metal species for the transfer hydrogenation of benzaldehyde. On the basis of this initial screening of metal triflates, we heterogenized Zr and Hf in UiO-66 and MOF-808 frameworks. We characterized their physicochemical characteristics, determined their MPV activities, and performed density functional theory to explain the reaction pathways.

3.1. Evaluation of the catalytic activity of catalysts for transfer hydrogenation of benzaldehyde

To identify the active metal species for MPV reaction, we screened 14 metal triflates with benzaldehyde as a reactant in 2-propanol at 100 °C for 3 h (**Fig. S2**). We chose benzaldehyde because it represented lignin-derived aldehyde. We found $Hf(OTf)_4$ had the highest benzyl alcohol selectivity of 56% at 90% benzaldehyde conversion after 3 h; whereas $Zr(OTf)_4$ exhibited 24% benzyl alcohol selectivity at 76% conversion.

3.2. Synthesis and characterization of Zr- and Hf-containing MOFs

Because $Hf(OTf)_4$ and $Zr(OTf)_4$ showed high selectivity to benzyl alcohol at high conversion, we heterogenized Hf and Zr species into UiO-66 and MOF-808 frameworks. To assess their physical and chemical properties, we characterized the synthesized MOFs by N_2 adsorption-desorption measurement, FTIR, TGA, XRD, DRIFTS, ICP-OES (**Fig. S3, Fig. S4, Table S2, Table S3**). The XRD and N_2adsorption-desorption of synthesized MOFs confirmed the formation of UiO-66 and MOF-808 structures. The ICP-OES results suggested that these MOFs had 26.3-31.6 wt.% Zr and 40.6-42.4 wt.% Hf. Together, the characteristics of these MOFs agreed well with previous reports (*see Supporting Information for detail*). The TGA profiles of these MOFs showed the typical three mass loss zones from physisorbed water, bound solvents, and degradation of frameworks. Moreover, the TGA results suggested that these Zr- and Hf-MOFs were stable up to 250 °C.

An ideal UiO-66 contains four Brønsted acidic sites (μ_3−OH) per cluster and no Lewis acidic sites [60,61]. To determine the Brønsted acidity of UiO-66, we measured the pH of the filtrate after suspending MOFs in methanol (Table 1). The pH after suspension with hydrated and dehydrated MOF-808(Zr) and MOF-808(Hf) did not change compared with the blank, which suggested that MOF-808(Zr) and MOF-808(Hf) possessed only Lewis acidity. These results agreed with previous observations [34]. Interestingly, suspension of dehydrated UiO-66 in methanol produced a decrease in pH from 6.0 to 4.2-4.3, which indicated the Brønsted acidity of UiO-66. Furthermore, the suspension of hydrated UiO-66 in methanol caused a further decrease in pH to 2.7-2.9, which indicated that bound water increased Brønsted acid strength of UiO-66. This increase in Brønsted acidity of hydrated UiO-66 stemmed

Table 1
pH values of hydrated and dehydrated MOFs suspended in methanol.

Catalyst\pH	Hydrated[a]	Dehydrated[b]
UiO-66(Zr)	2.7	4.2
UiO-66(Hf)	2.9	4.3
MOF-808(Zr)	5.8	6.0
MOF-808(Hf)	5.9	6.0
Methanol (blank)	6.1	-

[a] pH of a stirred suspension of 8 mg of MOF particles in 24 mL of methanol at 25 °C. [b]MOFs were dried at 150 °C for 12 h under vacuum before suspension in methanol.

from strongly polarized bound water on the coordinatively unsaturated sites (CUS) of UiO-66 [34]. Moreover, after removing hydrated solids, the pH of methanol was ~5.8-6.0, which suggested that the Brønsted acidic proton was on the surface of hydrated solids.

Next, we performed DRIFTS to measure the acid properties of MOFs. DRIFT spectra of MOF-808(Hf) and MOF-808(Zr) confirmed their Lewis acidic properties (**Fig. S4**). The UiO-66 MOF showed a weak band at 1070 cm^{-1}, which suggested that UiO-66 had little Lewis acidity. We postulated that the weak band at 1070 cm^{-1} came from defect formation during the MOF synthesis. To determine the amount of defects in synthesized UiO-66, we performed TGA on the MOFs and compared the results with the theoretical amount of linkers in ideal UiO-66 (**Fig. S5, Table S4**, *see Supporting Information for detail*). The defect sites of synthesized UiO-66(Zr) constituted 8.8%, in agreement with the reported value of 9.5% [34]. The calculated defect site of synthesized UiO-66(Hf) was 21.5%, in agreement with the reported TGA profile [62]. The defect sites of UiO-66(Zr) corroborated the occurrence of a weak Lewis acid peak at 1070 cm^{-1} (**Fig. S4**). These results agreed with findings by Cirujano et al. [52] and Guarinos et al. [34], which showed that bound water molecules on the defective Zr^{4+} sites of UiO-66 induced Brønsted acidity from strongly polarized bound H_2O molecules and corroborated the large decrease in pH induced by hydrated UiO-66. Overall, our results suggested that the MOF-808 had only Lewis acid sites, whereas UiO-66 had a mixture of Brønsted and Lewis acid sites. Moreover, the Lewis acid sites of UiO-66 were not stable because they could turn into Brønsted acid sites in the presence of moisture. Thus, to precisely control the content of Brønsted and Lewis acid sites in UiO-66 catalysts, it is important to handle them in a controlled environment (i.e., glove box).

3.3. *Catalytic activity of Zr- and Hf-containing MOFs for benzaldehyde conversion*

To evaluate their catalytic activity, we tested the Zr- and Hf-containing MOFs for benzaldehyde conversion through transfer hydrogenation during 3 h at the same metal loading. The control (no added catalyst) showed <20% benzaldehyde conversion without any benzyl alcohol formed. We used $Zr(OTf)_4$ and $Hf(OTf)_4$ as controls for Lewis acid catalyst. All catalysts showed a progressive increase in benzaldehyde conversion and benzyl alcohol selectivity during 3 h (Fig. 1**A and** 1**B**). Catalyst $Hf(OTf)_4$ had 56% selectivity to benzyl alcohol at 90% conversion after 3 h, greater than the 24% selectivity at 76% conversion for $Zr(OTf)_4$. Interestingly, UiO-66(Zr) and UiO-66(Hf) showed similar catalytic behavior to catalysis by $Zr(OTf)_4$ and $Hf(OTf)_4$. MOF-808(Zr) and MOF-808(Hf) outperformed UiO-66(Zr) and UiO-66 (Hf). Moreover, Zr- and Hf-containing MOF-808 reached 90-95% selectivity to benzyl alcohol at 98-99% conversion after 2 h. The higher benzaldehyde conversion and selectivity to benzyl alcohol of MOF-808 suggested that Zr and Hf metal sites in the MOF-808 framework were more active and selective than triflate salts and UiO-66. These metal sites were not active for hydrogenation using molecular H_2 (*see Supplementary Materials for detail,* **Fig. S6**).

To evaluate the quality of active sites, we plotted benzaldehyde conversion versus benzyl alcohol selectivity (Fig. 1**C**). As expected, the selectivity to benzyl alcohol was in the order of MOF-808(Hf) > MOF-808(Zr) > UiO-66(Hf) ≅ $Hf(OTf)_4$ > UiO-66(Zr) ≅ $Zr(OTf)_4$. At similar benzaldehyde conversion, MOF-808(Hf) showed higher selectivity to benzyl alcohol compared with MOF-808(Zr). These results suggested that (1) Brønsted and Lewis acid sites were active for benzaldehyde conversion, and (2) Lewis acidic MOF-808 catalysts were more selective to benzyl alcohol than were triflate salts and UiO-66 catalysts.

Because our synthesized UiO-66 catalysts had both Brønsted and Lewis acidities, we used Brønsted acidic H_2SO_4 as a control to decouple the activities of Brønsted and Lewis acidity for transfer hydrogenation (**Fig. S7**). With benzaldehyde as a reactant, we did not observe benzyl alcohol as a reaction product. The H_2SO_4 catalyst was active for benzaldehyde conversion. However, it was not selective to benzyl alcohol. Instead, we observed acetal as a product. Moreover, brown substances appeared in the reaction solution; we postulated that the brown

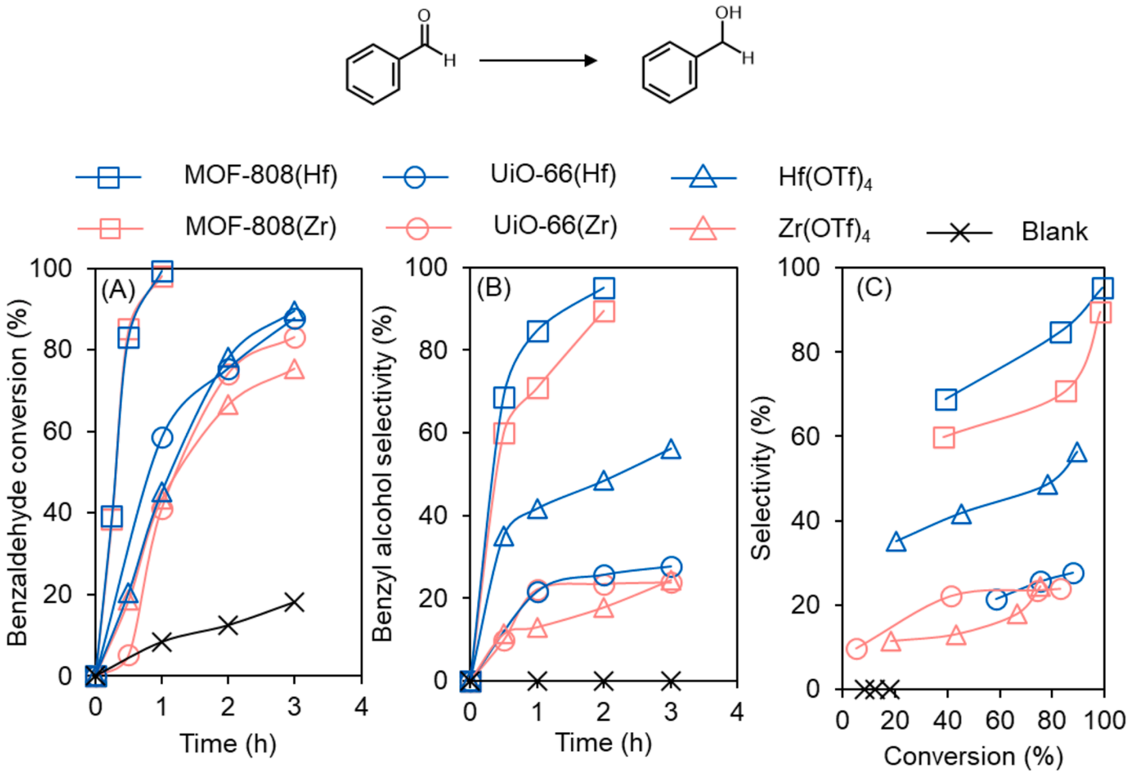

Fig. 1. Catalytic activity of selected Zr- and Hf-containing catalysts; time on stream of benzaldehyde conversion (A), benzyl alcohol selectivity (B), and conversion over selectivity (C). Reaction condition: 1 wt.% benzaldehyde in 2-propanol, catalyst loading = 3 mol.% metal, 100 °C, 0.5-3.0 h.

substances were degradation products (coke). Next, we used benzyl alcohol as a reactant (**Fig. S8**). The control, (no added catalyst) showed <20% conversion of benzyl alcohol without any products. Adding H_2SO_4 catalyst yielded 2-benzyloxypropane as a major reaction product, which suggested that H_2SO_4 catalyzed etherification of benzyl alcohol with 2-propanol over Brønsted acidic H_2SO_4. Also, we again observed brown substances suggestive of degradation products (coke). Overall, our results indicated that Brønsted acids promoted undesired side reactions (forming acetals and degradation of reactants, intermediates, and reaction products).

Although ideal UiO-66 catalysts have only Brønsted acid sites, defect formation is unavoidable during UiO-66 synthesis. Our synthesized UiO-66(Zr) contained ~8.8% missing linkers, which acted like Lewis acids. Similarly, the synthesized UiO-66(Hf) catalyst contained ~3.1% defect sites. Although these defect sites catalyzed the transfer hydrogenation of benzaldehyde to benzyl alcohol, the selectivity to benzyl alcohol was low (27%) at 88% conversion. The low selectivity stemmed from (1) a low number of Lewis acidic sites and (2) the transformation of Lewis acid sites into Brønsted acid sites, which promoted unwanted side reactions.

To further substantiate the foregoing claim, we synthesized UiO-66 (Hf) with added formic acid as a modulator and formed modulated UiO-66(Hf). The added formic acid during MOF synthesis created defect sites in the form of missing linkers. As expected, our calculation from TGA profile demonstrated that modulated UiO-66(Hf) had 21.5% defect sites (**Table S4**). In addition, the modulated UiO-66(Hf) had 47% selectivity to benzyl alcohol after 3 h compared with 27% from unmodulated UiO-66(Hf) (**Fig. S9**). These results suggested that adding Lewis acidic sites to UiO-66(Hf) enhanced the selectivity to benzyl alcohol.

3.4. *Density functional theory proposed mechanism of transfer hydrogenation of benzaldehyde by MOF-808 and UiO-66*

To explain the high catalytic activity of Zr- and Hf-containing MOF-808 for transfer hydrogenation of benzaldehyde with 2-propanol, we performed density functional theory (DFT) calculations [65]. Our calculations revealed that transfer hydrogenation of benzaldehyde by Zr- and Hf-containing MOFs followed the Meerwein–Ponndorf–Verley (MPV) two simultaneous elementary steps (Fig. 2): (1) hydrogen transfer from 2-propanol (alcohol) to benzaldehyde (reactant) to form intermediate (co-Ads to Int) and (2) formation of benzyl alcohol as a reaction product (Int to Prod). Initially, the 2-propanol and benzaldehyde molecules interacted on each open site of the M^{4+}-O^{2-} of the metal clusters in MOF-808(M= Zr or Hf) (co-Ads). In the transition state (TS1), the oxygen (O) of the surface hydroxide group of MOFs severed the O-H bond of 2-propanol and simultaneously enabled the hydrogen transfer (H1) from the C2 of 2-propanol to the carbonyl C1 of benzaldehyde. After the TS1, the reaction proceeded with the formation of benzyl alkoxide intermediate, acetone, and water molecules (Int). Finally, benzyl alcohol (product) is formed by the hydrogenation of benzyl alkoxide in the transition state (TS2). The TS2 involved the concerted O-H2 bond breaking and the formation of the O1-H2 bond. In contrast to our findings, Rojas-Buzo et al. [35] found that MOF-808(Hf) catalyzed direct transfer hydrogenation.

Fig. 2 shows the optimized structures for the MPV reaction, and the relative free energies calculated for Zr- and Hf-containing MOF-808. The co-adsorption free energies of benzaldehyde and 2-propanol were –11.7 and –10.9 kcal/mol for MOF-808(Zr) and MOF-808(Hf), respectively (co-Ads, Fig. 2). The binding energy of MOF-808(Zr) was greater than that of MOF-808(Hf) because charge transfer from molecules to the active site of MOF-808(Zr) was 0.191e, greater than the 0.188e charge transfer of MOF-808(Hf). The activation energy of step 1 (E_{a1}) was 20.1 and 17.8 kcal/mol for of Zr- and Hf-containing MOF-808, greater than the activation energy of step 2 (no barriers with E_{a2} = -1.3 and -2.0 kcal/mol for MOF-808(Zr) and MOF-808(Hf), respectively). These results suggested that the hydrogen transfer (step 1) was the rate-determining step. To explain the difference between MPV activity of Zr- and Hf-containing MOF-808, we further calculated the different amount of charge transfer (DCT) from the catalytic sites to the adsorbed benzaldehyde molecule between the adsorption and transition state complexes. The DCTs of MOF-808(Zr) and MOF-808(Hf) were 0.462 and

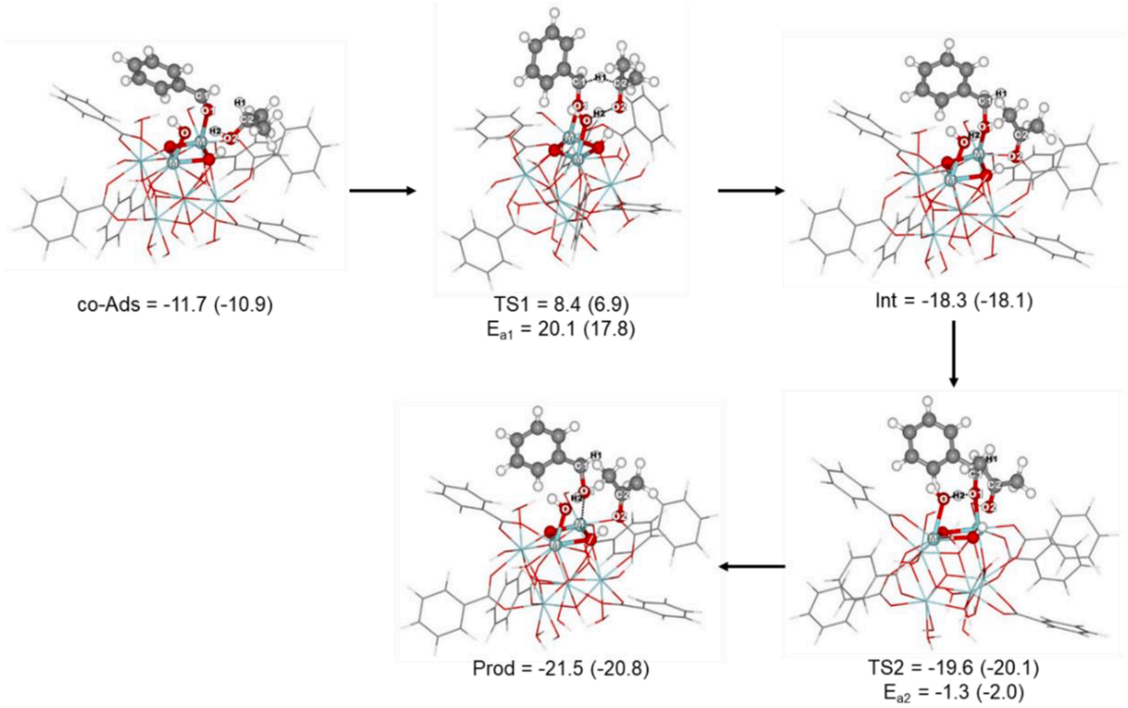

Fig. 2. Proposed mechanism of MPV reduction of benzaldehyde with 2-propanol to produce benzyl alcohol by Zr- and Hf-containing MOF-808. Values in parentheses are the free energies of MOF-808(Hf) in kcal/mol. Co-Ads = co-adsorption of benzaldehyde and 2-propanol molecules, TS1 and TS2 = transition state of step 1 and 2, Int = intermediate, Prod = product, and E_{a1} and E_{a1} = activation energies of step 1 and 2.

0.471e, respectively. The higher DCT value of MOF-808(Hf) resulted in a lower activation energy barrier compared with MOF-808(Zr) (E_{a1} of MOF-808(Hf) $<$ E_{a1} of MOF-808(Zr)), which corroborated the activation barriers shown in Fig. 2. With a low activation energy barrier, MOF-808 (Hf) weakened the C=O carbonyl bond of benzaldehyde during the charge transfer process. It enhanced the ability of the C1 carbon atom to accept the H1 hydrogen (transferred) from 2-propanol. Overall, these results suggested that (1) Lewis acidic MOF-808 catalyzed transfer hydrogenation by MPV, and (2) MOF-808(Hf) was more active at MPV of benzaldehyde than MOF-808(Zr).

Unlike MOF-808, UiO-66 did not have Lewis acidic sites to activate the carbonyl group of benzaldehyde for the MPV [35]. Therefore, we postulated that the Brønsted acid sites of UiO-66(Hf) participated in the benzaldehyde conversion. To test this hypothesis, we investigated the co-adsorption of benzaldehyde and 2-propanol on Hf (co_Ads_a) and Brønsted sites (co_Ads_b) on UiO-66(Hf) (**Fig. S10).** The calculated energy of the co-adsorption on Hf was 3.8 kcal/mol (endothermic), whereas the co-adsorption of benzaldehyde and 2-propanol on the Brønsted site was -4.7 kcal/mol (exothermic); these energies suggested that Brønsted sites were the preferred sites for the co-adsorption, and the reaction proceeded without intermediates. Fig. 3 shows a proposed benzaldehyde conversion by UiO-66(Hf). The reaction proceeded by the co-adsorption of benzaldehyde and 2-propanol over the Brønsted site of UiO-66(Hf) (co-Ads). At the transition state (TS), the benzaldehyde was simultaneously hydrogenated at C1 and O1 atoms via the hydrogen transfer from 2-propanol to form the benzyl alcohol product (Prod). The activation energy barrier was 28.4 kcal/mol, significantly greater than the 17.8 kcal/mol (Fig. 2) activation energy for MOF-808(Hf). These results suggested that (1) Brønsted sites of UiO-66(Hf) were active for transfer hydrogenation, which corroborated our experimental results that showed high benzaldehyde conversion (Fig. 1), and (2) the UiO-66 (Hf) Brønsted sites catalyzed the direct transfer hydrogenation.

3.5. *Proposed chemical pathway for Meerwein–Ponndorf–Verley reduction of benzaldehyde by MOF-808(Hf)*

On the basis of our experimental results, we proposed a chemical pathway for the MOF-808(Hf)-catalyzed MPV reduction of benzaldehyde to benzyl alcohol (Fig. 4). First, 2-propanol and benzaldehyde molecules are co-absorbed on MOF-808(Hf) and interact with the Hf^{4+}-O^{2-} of the Hf clusters. Next, acidic Hf^{4+} species activate the carbonyl groups in benzaldehyde. Then the reaction proceeds by a hydrogen transfer and 2-propanol O-H bond-breaking steps and forms the benzyl alkoxide intermediate, acetone, and water molecules. Finally, the benzyl alkoxide intermediate coordinated with the Hf metal center is transformed into benzyl alcohol.

3.6. *Transfer hydrogenation of selected carbonyl compounds with MOF-808(Hf)*

Because Lewis acidic MOF-808(Hf) was active and selective for transfer hydrogenation of benzaldehyde, we used MOF-808(Hf) with six carbonyl compounds with aromatic, furan, and aliphatic structure, namely, furfural (a), 5-methyl furfural (b), 5-(hydroxymethyl) furfural (c), cyclohexanone (d), acetophenone (e), and 2-hexanone (f) (Fig. 5). MOF-808(Hf) reduced these carbonyls to corresponding alcohols with >89% selectivity with minimal side reactions (e.g., coke formation) [66–69]. Interestingly, we obtained a low conversion (45.1%) of 5-methyl furfural (b). The low activity of MOF-808(Hf) on 5-methyl furfural (b) was due to steric hindrance and the presence of methyl group. The electron-donating nature of the methyl group in compound b increased electron density on the carbon atom of the carbonyl group. As a result, the attack of hydride ions on the carbonyl carbon was not favorable. Although one would expect a low conversion of 5-(hydroxymethyl) furfural (compound c) due to structural similarity to compound b, our results showed 86.1% conversion of compound c. We postulated that the OH group of compound c formed a hydrogen bond with the oxygen atom in the furan ring and decreased electron density on the carbon atom of the carbonyl group. Therefore, the activity of the carbonyl group for proton subtraction is enhanced. Together, these results suggested high selectivity of MOF-808(Hf) for transfer hydrogenation of carbonyl compounds.

3.7. *Stability and reusability of MOF-808 in transfer hydrogenation of benzaldehyde*

To evaluate the catalyst stability under the reaction condition, we performed filtration experiments by conducting the transfer hydrogenation using MOF-808(Hf) for 1 h at 100 °C, filtering the MOF-808(Hf) catalyst from the reaction mixture, and heating the filtrate under the same reaction condition (100 °C) for 4 h (Fig. 6**A**). We sampled the reaction mixture three times during the 3 h and measured benzaldehyde conversion and benzyl alcohol selectivity. The conversion of benzaldehyde slightly increased, whereas the selectivity to benzyl alcohol slightly decreased. One reason was that benzaldehyde and benzyl alcohol degraded at 100 °C, which corroborated our blank experiments of benzaldehyde (Fig. 1) and benzyl alcohol (**Fig. S8**).

The ability to recycle catalysts is important for their practical use. We recycled the MOF-808(Hf) by centrifugation and washing with ethyl acetate to remove the residual products, intermediates, and unreacted benzaldehyde. The catalyst was then dried in a vacuum oven at 130 °C to remove moisture and residual solvent. We selected this temperature based on our TGA results to minimize the decomposition of MOF-808. The MOF-808(Hf) catalyst maintained a high selectivity to benzyl alcohol (94%) with a slight decrease in benzaldehyde conversion (11%)

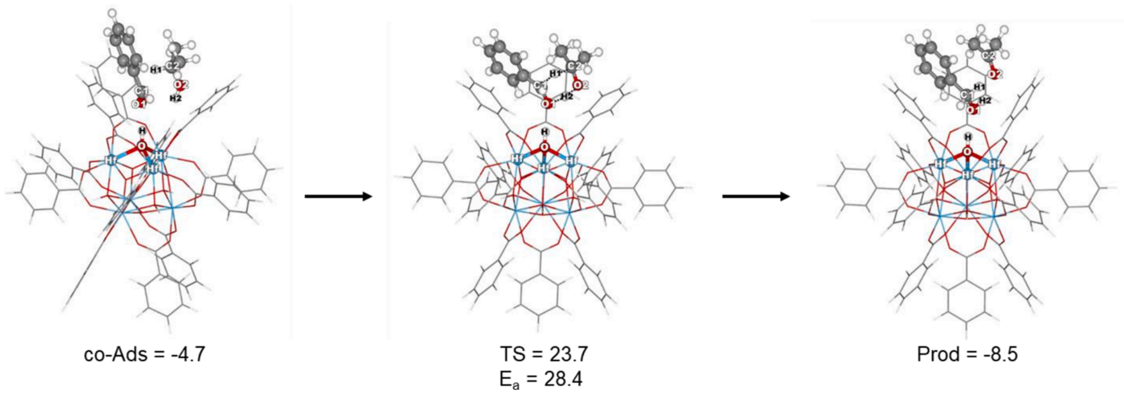

Fig. 3. Proposed mechanism of benzaldehyde reaction with 2-propanol over Brønsted acid sites in UiO-66(Hf) and free energies (kcal/mol). Co-Ads = co-adsorption of benzaldehyde and 2-propanol molecules, TS = transition state, Prod = product, and E_a = activation energy.

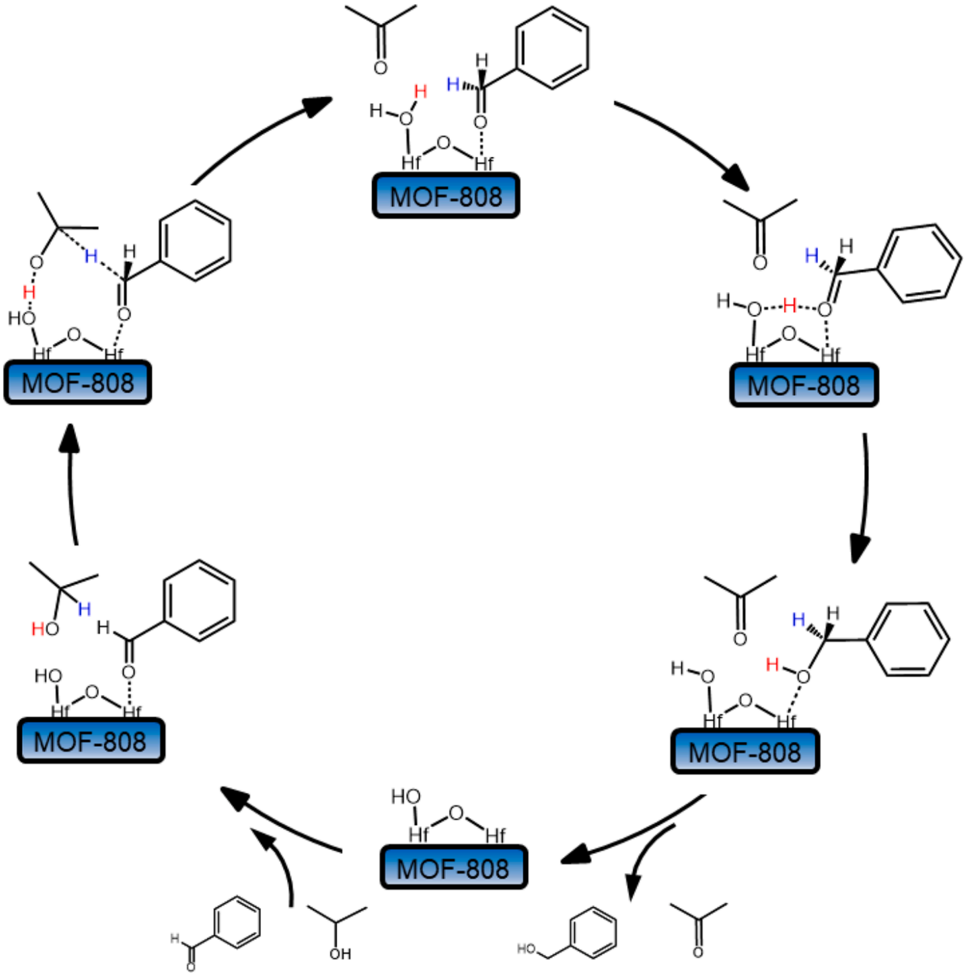

Fig. 4. Proposed chemical pathway for Meerwein–Ponndorf–Verley reduction of benzaldehyde with 2-propanol to benzyl alcohol by MOF-808(Hf).

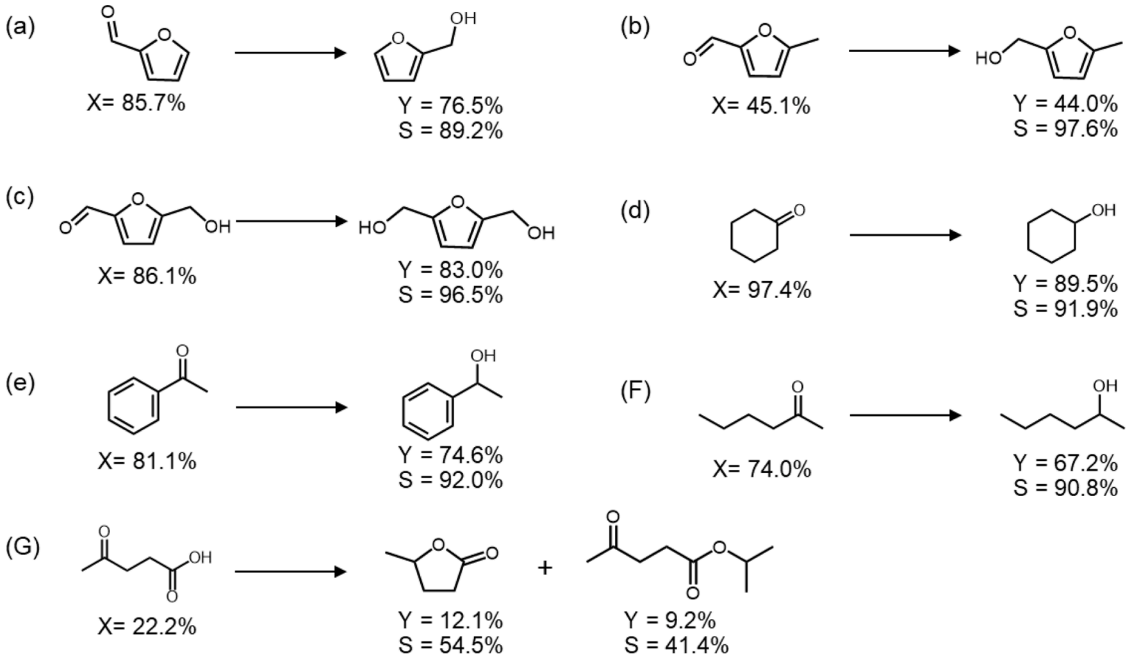

Fig. 5. Transfer hydrogenation of selected carbonyls by MOF-808(Hf). X, Y, and S indicate the conversion of aldehydes, yield of their corresponding alcohols, and selectivity, respectively. Reaction condition. 1 wt.% carbonyl compound in 2-propanol, catalyst loading = 3 mol.% Hf, 100 °C, 1 h.

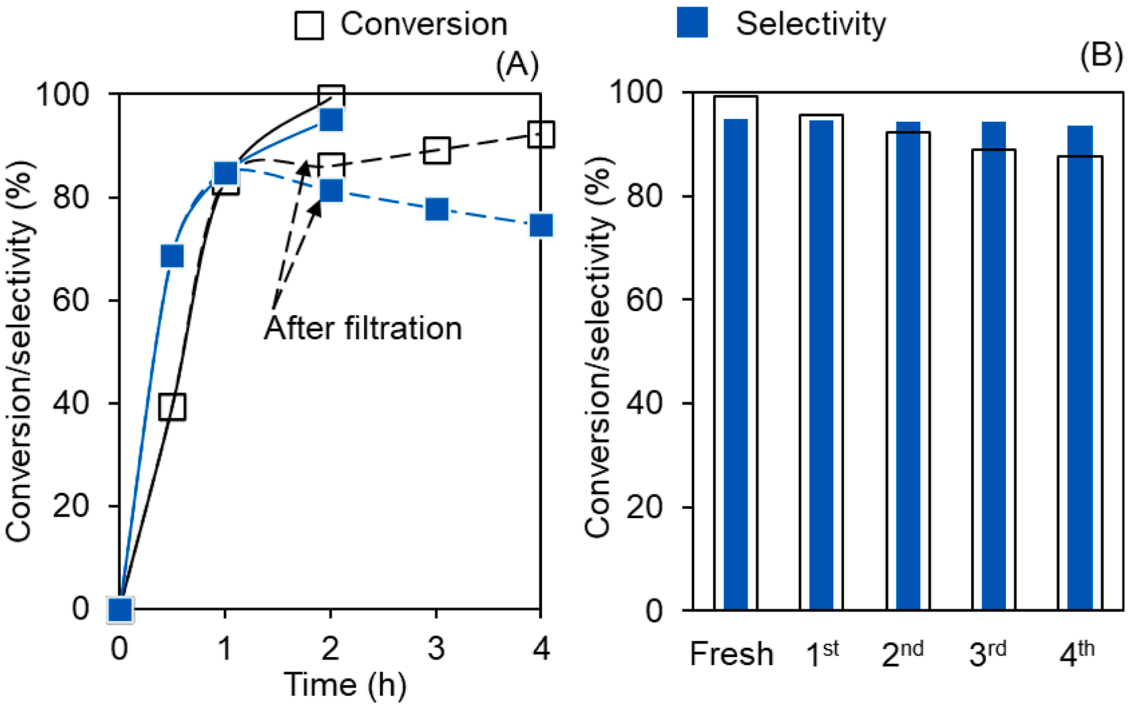

Fig. 6. Stability and reusability of MOF-808(Hf) for the MPV reduction of benzaldehyde to benzyl alcohol by filtration test at 100 °C (A) and recycle of MOF-808(Hf) catalyst at 100 °C, 2 h (B). Reaction condition. 1 wt.% benzaldehyde in 2-propanol, catalyst loading = 3 mol.% metal (Hf).

over four cycles (Fig. 6**B**). Further, we used ICP-OES, XRD, and FTIR to characterize the spent MOF-808(Hf) catalyst after the 4th reuse cycle (**Fig. S11**). The hafnium content of the spent catalyst, measured by ICP-OES, was 37.3 wt.%, ~8% lower than that of fresh catalysts (40.6 wt.%). This decrease in hafnium content after 4th reuse cycle was proportional to the drop in conversion of benzaldehyde, which suggested that metal leaching was the deactivation mechanism of MOF-808(Hf). However, this metal leaching was not significant as evidenced by a high selectivity to benzyl alcohol (94%) at 88% benzaldehyde conversion after 4 cycles. In a like manner, the XRD and FTIR spectra of the reused catalyst exhibited chemical structure and functionality similar to fresh MOF-808 (Hf) (**Fig. S11**). These filtration and characterization results suggested catalyst stability under the present experimental conditions. Overall, MOF-808(Hf) maintained high selectivity to benzyl alcohol for all the cycles and structural integrity after (at least) four recycles.

4. Discussion

The challenge in catalytic transfer hydrogenation is developing active, selective, and reusable catalysts [18,19]. We investigated the catalytic performance of Zr- and Hf-containing MOF-808 and UiO-66 catalysts for the transfer hydrogenation of carbonyl compounds to their corresponding alcohols. The Lewis acidic MOF-808(Hf) was the most active for transfer hydrogenation of benzaldehyde and the most selective to corresponding alcohols, with 95% selectivity to benzyl alcohol at 99% conversion of benzaldehyde. Our combined experimental and computational results explained the effects of the metal and acid sites on the chemical pathway of transfer hydrogenation of carbonyl compounds and the stability of products.

Our most significant finding was the detailed mechanism of MOF-808-catalyzed MPV and UiO-66-catalyzed direct transfer hydrogenation. Lewis acidic MOF-808 underwent the MPV pathway of carbonyl compounds, which was active and selective to corresponding alcohols, whereas UiO-66 could not catalyze transfer hydrogenation selectively. Although our calculations showed that Brønsted acid sites of UiO-66 catalyzed direct transfer hydrogenation of carbonyl compounds, the high activation energy barrier made catalysis difficult. Moreover, Brønsted acids promoted the unwanted formation of acetals and degradation products. Thus, the selective transfer hydrogenation of carbonyl compounds by UiO-66 relied on the presence of Lewis acids from the generation of defects during MOF synthesis. For example, our synthesized UiO-66 contained ~8.8% missing linkers, which indicated that each missing linker molecule (terephthalic acid) created two coordinatively unsaturated Zr^{4+} that acted like Lewis acids. Our calculation of missing linkers implied that only ~18% of the total zirconium ions in UiO-66(Zr) participated in the MPV reaction. The rest of the zirconium ions initiated the direct transfer hydrogenation and unwanted side reactions (formation of hemiacetals and degradation products). Thus, we observed a low selectivity of benzyl alcohol products at a high benzaldehyde conversion. Conversely, all Zr^{4+} ions in MOF-808 participated in MPV of carbonyl compounds. As a result, MOF-808 provided a high selectivity of corresponding alcohols at a high conversion, which agreed with the high activity and selectivity of MOF-808 for the reduction of carbonyl compounds [35,41,71,72].

Another significant finding was a lower activation energy of the transfer hydrogenation by MOF-808(Hf) compared with MOF-808(Zr). Our quantum calculations revealed that the charge transfer from Hf active sites to the benzaldehyde molecule was higher than that of Zr sites and resulted in lower activation energy. These findings implied that the charge transfer process was crucial in activating the C=O bond, and the charge transfer facilitated the transferred hydrogen from the -OH group of 2-propanol (H1). We postulated that this high charge transfer of MOF-808(Hf), compared with MOF-808(Zr), resulted in a greater Lewis acidity of Hf sites compared with Zr sites. As a result, MOF-808(Hf) had a high activity for transfer hydrogenation relative to MOF-808(Zr). These results agreed with findings by Koehle et al. [73] and Sittiwong et al. [74]. They observed that Hf active sites in Lewis acidic β-zeolites and UiO-66 MOFs provided a lower activation barrier than did Zr sites in catalytic transfer hydrogenation of furfural to furfuryl alcohol.

Our findings advance understanding of the function of Lewis and Brønsted acid sites of Hf- and Zr-containing MOF-808 and UiO-66 MOFs and reaction pathways for transfer hydrogenation. Moreover, the MOF synthesis procedures are simple, environmentally friendly, and scalable compared with the preparation of conventional selective catalysts for transfer hydrogenation, such as Hf-, Zr-, and Sn-containing zeolites [31–33]. Although defective UiO-66(Hf) was not selective to transfer hydrogenation, the knowledge gained from the defects-induced Brønsted acidity of UiO-66 will enable tuning the Brønsted acid strength and balance Lewis/Brønsted acid ratio for various organic reactions, such as dehydration [75], isomerization [76], condensation [77–80], and acetalization [81] and cascade reactions that require both Lewis and Brønsted acidities, such as cellulose conversion to 5-hydroxymethylfurfural [75], lactic acid [76,82], and levulinic acid [83].

5. Conclusion

Catalytic transfer hydrogenation is a promising approach for upgrading biomass-derived molecules to high-value chemicals. This study described the mechanism of transfer hydrogenation of benzaldehyde by Hf- and Zr-containing MOF-808 and UiO-66 metal-organic frameworks (MOFs). Although these MOFs have demonstrated their transfer hydrogenation ability, the effect of metal sites and acid sites on the chemical pathway was unknown. Our results demonstrated that Hf- and Zr-containing MOF-808 catalysts enabled selective MPV reduction of carbonyl compounds to corresponding alcohols. Moreover, MOF-808 (Hf) was more active and selective to transfer hydrogenation because Hf active sites had a lower activation energy barrier compared with Zr sites. Although creating (Lewis acidic) defects in UiO-66 enhanced its selective transfer hydrogenation, the defects induced Brønsted acidity in the presence of water, which decreased the selectivity because of side reactions. Thus, caution must be exercised in creating and handling defective UiO-66 catalysts so as to control the type of acid sites. Future studies will focus on tuning the Brønsted and Lewis acidity of these MOFs, reversibility of the defects-induced Brønsted acidity, and long-term stability.

CRediT authorship contribution statement

Mohammad Shahinur Rahaman: Conceptualization, Formal analysis, Investigation, Validation, Writing – original draft. **Sarttrawut Tulaphol:** Conceptualization, Formal analysis, Visualization. **Md. Anwar Hossain:** Investigation. **Matthew C. Mulvehill:** Investigation. **Joshua M. Spurgeon:** Supervision. **Thana Maihom:** Conceptualization, Formal analysis, Methodology, Writing – review & editing. **Noppadon Sathitsuksanoh:** Conceptualization, Funding acquisition, Methodology, Project administration, Supervision, Writing – review & editing.

Declaration of Competing Interest

The authors declare that they have no known competing financial interests or personal relationships that could have appeared to influence the work reported in this paper.

Acknowledgment

A part of this material is based upon work supported by the National Science Foundation under Cooperative Agreement No. 1355438 and Internal Research Grant, Office of the Executive Vice President for Research, University of Louisville. This work was performed in part at the Conn Center for Renewable Energy Research at the University of Louisville, which belongs to the National Science Foundation NNCI KY Manufacturing and Nano Integration Node, supported by ECCS-1542174. T.M. acknowledges support from the Office of the Permanent Secretary, Ministry of Higher Education, Science, Research and Innovation, Thailand (Grant No. RGNS 63-038). The authors would like to thank Ashten Molley, Kyle Mills, Sandesh Uttarwar, and Francois Nkurunziza from University of Louisville for their help in performing selected MPV experiments. The authors would like to thank Dr. Howard Fried for his valuable comments and suggestions on the manuscript.

Supplementary materials

Supplementary material associated with this article can be found, in the online version, at doi:10.1016/j.mcat.2022.112247.

References

[1] H.K. Sharma, C. Xu, W. Qin, Waste Biomass Valorizat. 10 (2019) 235–251.
[2] D.R. Cohn, L. Bromberg, J.B. Heywood, (2006).
[3] A. Galletti, C. Antonetti, V. De Luise, M. Martinelli, Green Chem 14 (2012) 688–694.
[4] R. Alamillo, M.G. Tucker, M. Chia, Y. Pagán-Torres, J. Dumesic, Green Chem 14 (2012) 1413–1419.
[5] H. Xia, C. Chen, P. Liu, M. Zhou, J. Jiang, Sustain. Energy Fuels 4 (2020) 5709–5720.
[6] M.J. Ahmed, B.H. Hameed, J. Taiwan Inst. Chem. Eng. 96 (2019) 341–352.
[7] S. Li, X. Wang, X. Liu, G. Xu, S. Han, X. Mu, Catal. Commun. 61 (2015) 92–96.
[8] Z. Yan, L. Lin, S. Liu, Energy Fuels 23 (2009) 3853–3858.
[9] B.M. Matsagar, C.Y. Hsu, S.S. Chen, T. Ahamad, S.M. Alshehri, D.C.W. Tsang, K.C.W. Wu, Sustain. Energy Fuels 4 (2020) 293–301.
[10] Y. Nakagawa, K. Tomishige, Catal. Commun. 12 (2010) 154–156.
[11] J. Ohyama, A. Esaki, Y. Yamamoto, S. Arai, A. Satsuma, RSC Adv., 3 (2013) 1033–1036.
[12] K. Hengst, D.M. Ligthart, D.E. Doronkin, K.M. Walter, W. Kleist, E.J.M. Hensen, J. Grunwaldt, Ind. Eng. Chem. Res. 56 (2017) 2680–2689.
[13] I. Obregón, E. Corro, U. Izquierdo, J. Requies, P.L. Arias, Chin. J. Catal. 35 (2014) 656–662.
[14] J.Y. Yeh, B.M. Matsagar, S.S. Chen, H.L. Sung, D.C.W. Tsang, Y.P. Li, K.C.W. Wu, J. Catal. 390 (2020) 46–56.
[15] M. Balakrishnan, E.R. Sacia, A.T. Bell, Green Chem 14 (2012) 1626–1634.
[16] H. Cai, C. Li, A. Wang, T. Zhang, Catal. Today 234 (2014) 59–65.
[17] W. Jin, L. Pastor-Pérez, J. Yu, J. Odriozola, S. Gu, T. Reina, Curr. Opin. Green Sustain. Chem. 23 (2020) 1–9.
[18] P. Panagiotopoulou, D. Vlachos, Appl. Catal. A. 480 (2014) 17–24.
[19] P. Panagiotopoulou, N. Martin, D.G. Vlachos, J. Mol. Catal. A: Chem. 392 (2014) 223–228.
[20] A. Corma, M.E. Domine, L. Nemeth, S. Valencia, J. Am. Chem. Soc. 124 (2002) 3194–3195.
[21] R. Johnstone, A. Wilby, I. Entwistle, Chem. Rev. 85 (1985) 129–170.
[22] R. Assary, L. Curtiss, J. Dumesic, ACS Catal., 3 (2013) 2694–2704.
[23] Y. Injongkol, T. Maihom, P. Treesukul, J. Sirijaraensre, B. Boekfa, J. Limtrakul, Phys. Chem. Chem. Phys. 19 (2017) 24042–24048.
[24] B. Johnson, J. Di Iorio, Y. Román-Leshkov, J. Catal. 404 (2021) 607–619.
[25] J. Lewis, S. Van de Vyver, A. Crisci, W. Gunther, V. Michaelis, R. Griffin, Y. Román-Leshkov, ChemSusChem 7 (2014) 2255–2265.
[26] A. Prasertsab, T. Maihom, M. Probst, C. Wattanakit, J. Limtrakul, Inorg. Chem. 57 (2018) 6599–6605.
[27] B. Tang, S. Li, W.-C. Song, E.-C. Yang, X.-J. Zhao, N. Guan, L. Li, ACS Sustain. Chem. Eng. 7 (2019) 16329–16343.
[28] A. Corma, M. Domine, L. Nemeth, S. Valencia, J. Am. Chem. Soc. 124 (2002) 3194–3195.
[29] A. Corma, M.E. Domine, S. Valencia, J. Catal. 215 (2003) 294–304.
[30] W. Hu, Y. Wan, L. Zhu, X. Cheng, S. Wan, J. Lin, Y. Wang, ChemSusChem 10 (2017) 4715–4724.
[31] W. van der Graaff, C. Tempelman, E. Pidko, E. Hensen, Catal. Sci. Technol. 7 (2017) 3151–3162.
[32] C.-C. Chang, Z. Wang, P. Dornath, H. Je Cho, W. Fan, RSC Adv., 2 (2012) 10475–10477.
[33] C. Hammond, S. Conrad, I. Hermans, Angew. Chem. Int. Ed. 51 (2012) 11736–11739.
[34] J. Guarinos, F. Cirujano, A. Rapeyko, F. Llabrés i Xamena, Mol. Catal. 515 (2021), 111925.
[35] S. Rojas-Buzo, P. García-García, A. Corma, ChemSusChem 11 (2018) 432–438.
[36] Y. Lin, Q. Bu, J. Xu, X. Liu, X. Zhang, G.-P. Lu, B. Zhou, Mol. Catal. 502 (2021), 111405.
[37] H.-H. Mautschke, F. Drache, I. Senkovska, S. Kaskel, F. Llabrés i Xamena, Catal. Sci. Technol. 8 (2018) 3610–3616.
[38] A. Valekar, M. Lee, J. Yoon, J. Kwak, D.-Y. Hong, K.-R. Oh, G.-Y. Cha, Y.-U. Kwon, J. Jung, J.-S. Chang, ACS Catal 10 (2020) 3720–3732.
[39] S. Rojas-Buzo, P. García-García, A. Corma, Green Chem 20 (2018) 3081–3091.
[40] Y. Kuwahara, H. Kango, H. Yamashita, ACS Sustainable Chem. Eng. 5 (2017) 1141–1152.
[41] A.H. Valekar, M. Lee, J.W. Yoon, J. Kwak, D. Hong, K. Oh, G. Cha, Y. Kwon, J. Jung, J. Chang, ACS Catal 10 (2020) 3720–3732.
[42] T. Wang, A. Hu, G. Xu, C. Liu, H. Wang, Y. Xia, Catal. Lett. 149 (2019) 1845–1855.
[43] M. Qiu, T. Guo, R. Xi, D. Li, X. Qi, Appl. Catal., A 602 (2020), 117719.
[44] A.H. Valekar, K. Cho, S.K. Chitale, D. Hong, G. Cha, U. Lee, D.W. Hwang, C. Serre, J. Chang, Y.K. Hwang, Green Chem 18 (2016) 4542–4552.
[45] Z. Cai, W. Li, F. Wang, X. Zhang, J. Taiwan Inst. Chem. Eng. 93 (2018) 374–378.
[46] E. Plessers, D.E. De Vos, M.B. Roeffaers, J. Catal. 340 (2016) 136–143.
[47] Z. Ma, C. Li, H. Fan, J. Wan, Y. Luo, B.-G. Li, Ind. Eng. Chem. Res. 56 (2017) 14089–14100.
[48] M.J. Cliffe, W. Wan, X. Zou, P.A. Chater, A.K. Kleppe, M.G. Tucker, H. Wilhelm, N.P. Funnell, F. Coudert, A.L. Goodwin, Nat. Commun. 5 (2014) 1–8.

[49] A.I. Osman, J.K. Abu-Dahrieh, D.W. Rooney, S.A. Halawy, M.A. Mohamed, A. Abdelkader, Appl. Catal., B 127 (2012) 307–315.

[50] D. Yu, M. Wu, Q. Hu, L. Wang, C. Lv, L. Zhang, J. Hazard. Mater. 367 (2019) 456–464.

[51] A. Herbst, A. Khutia, C. Janiak, Inorg. Chem. 53 (2014) 7319–7333.

[52] F. Cirujano, F. Llabrés i Xamena, J. Phys. Chem. Lett. 11 (2020) 4879–4890.

[56] M.R. Momeni, C.J. Cramer, ACS Appl. Mater. Interfaces 10 (2018) 18435–18439.

[57] Y. Zhao, D.G. Truhlar, Acc. Chem. Res. 41 (2008) 157–167.

[58] M. Frisch, G. Trucks, H. Schlegel, G. Scuseria, M. Robb, J. Cheeseman, G. Scalmani, V. Barone, G. Petersson, H. Nakatsuji, in, Gaussian, Inc. Wallingford, CT, 2016.

[59] A. Reed, L. Curtiss, F. Weinhold, Chem. Rev. 88 (1988) 899–926.

[60] V. Bakuru, S. Churipard, S. Maradur, S. Kalidindi, Dalton Trans., 48 (2019) 843-847.

[61] X. Feng, J. Hajek, H. Jena, G. Wang, S. Veerapandian, R. Morent, N. De Geyter, K. Leyssens, A. Hoffman, V. Meynen, J. Am. Chem. Soc. 142 (2020) 3174–3183.

[62] B. Villoria-del-Álamo, S. Rojas-Buzo, P. García García, A. Corma, Chem. Eur. J. 27 (2020) 4588–4598.

[65] A.S. Lawrence, B. Sivakumar, A. Dhakshinamoorthy, Mol. Catal. 517 (2022), 112042.

[66] S. Garg, D.K. Unruh, C. Krempner, Catal. Sci. Technol. 11 (2021) 211–218.

[67] B. Hernández, J. Iglesias, G. Morales, M. Paniagua, C. López-Aguado, J.L.G. Fierro, P. Wolf, I. Hermans, J.A. Melero, Green Chem 18 (2016) 5777–5781.

[68] J.D. Lewis, S. Van de Vyver, A.J. Crisci, W.R. Gunther, V.K. Michaelis, R.G. Griffin, Y. Román-Leshkov, ChemSusChem 7 (2014) 2255–2265.

[69] X. Tang, X. Zeng, Z. Li, W. Li, Y. Jiang, L. Hu, S. Liu, Y. Sun, L. Lin, ChemCatChem 7 (2015) 1372–1379.

[71] E. Plessers, G. Fu, C.Y.X. Tan, D.E. De Vos, M.B. Roeffaers, Catalysts 6 (2016) 104.

[72] Y. Lin, Q. Bu, J. Xu, X. Liu, X. Zhang, G. Lu, B. Zhou, Mol. Catal. 502 (2021), 111405.

[73] M. Koehle, R. Lobo, Catal. Sci. Technol. 6 (2016) 3018–3026.

[74] J. Sittiwong, S. Boonmark, W. Nunthakitgoson, T. Maihom, C. Wattanakit, J. Limtrakul, Inorg. Chem. 60 (2021) 4860–4868.

[75] M. Rahaman, S. Tulaphol, M. Hossain, J. Jasinski, N. Sun, A. George, B. Simmons, T. Maihom, M. Crocker, N. Sathitsuksanoh, Fuel 310 (2022), 122459.

[76] M. Rahaman, S. Tulaphol, K. Mills, A. Molley, M. Hossain, S. Lalvani, T. Maihom, M. Crocker, N. Sathitsuksanoh, ChemCatChem 14 (2022) e202101756.

[77] A. Das, N. Anbu, A. Dhakshinamoorthy, S. Biswas, Microporous Mesoporous Mater 284 (2019) 459–467.

[78] M.S. Rahaman, S. Tulaphol, M.A. Hossain, C.N. Evrard, L.M. Thompson, N. Sathitsuksanoh, Mol. Catal. 514 (2021), 111848.

[79] A. Das, N. Anbu, C. Gogoi, A. Dhakshinamoorthy, S. Biswas, Eur. J. Inorg. Chem. (2021) 3396–3403, 2021.

[80] A. Das, N. Anbu, P. Varalakshmi, A. Dhakshinamoorthy, S. Biswas, New J. Chem. 44 (2020) 10982–10988.

[81] M. Rahaman, T. Phung, M.A. Hossain, E. Chowdhury, S. Tulaphol, S. Lalvani, M. O'Toole, G. Willing, J. Jasinski, M. Crocker, N. Sathitsuksanoh, Appl. Catal., A (2020), 117369.

[82] M. Hossain, K. Mills, A. Molley, M. Rahaman, S. Tulaphol, S. Lalvani, J. Dong, M. Sunkara, N. Sathitsuksanoh, Appl. Catal. A. 611 (2021), 117979.

[83] S. Tulaphol, M.A. Hossain, M. Rahaman, L.-Y. Liu, T. Phung, S. Renneckar, N. Grisdanurak, N. Sathitsuksanoh, Energy Fuels 32 (2019) 1764–1772.